Sensor Package for Internal Detection In Extraterrestrial Regions (SPIDER)

New Mexico Institute of Mining and Technology

Advisor:

Mostafa Hassanalian, Ph.D.

Team Members:

Thomas Pierson, Undergraduate, Mechanical Engineering.

Riley Morris, Undergraduate, Mechanical Engineering.

Shawna Dodge, Undergraduate, Mechanical Engineering.

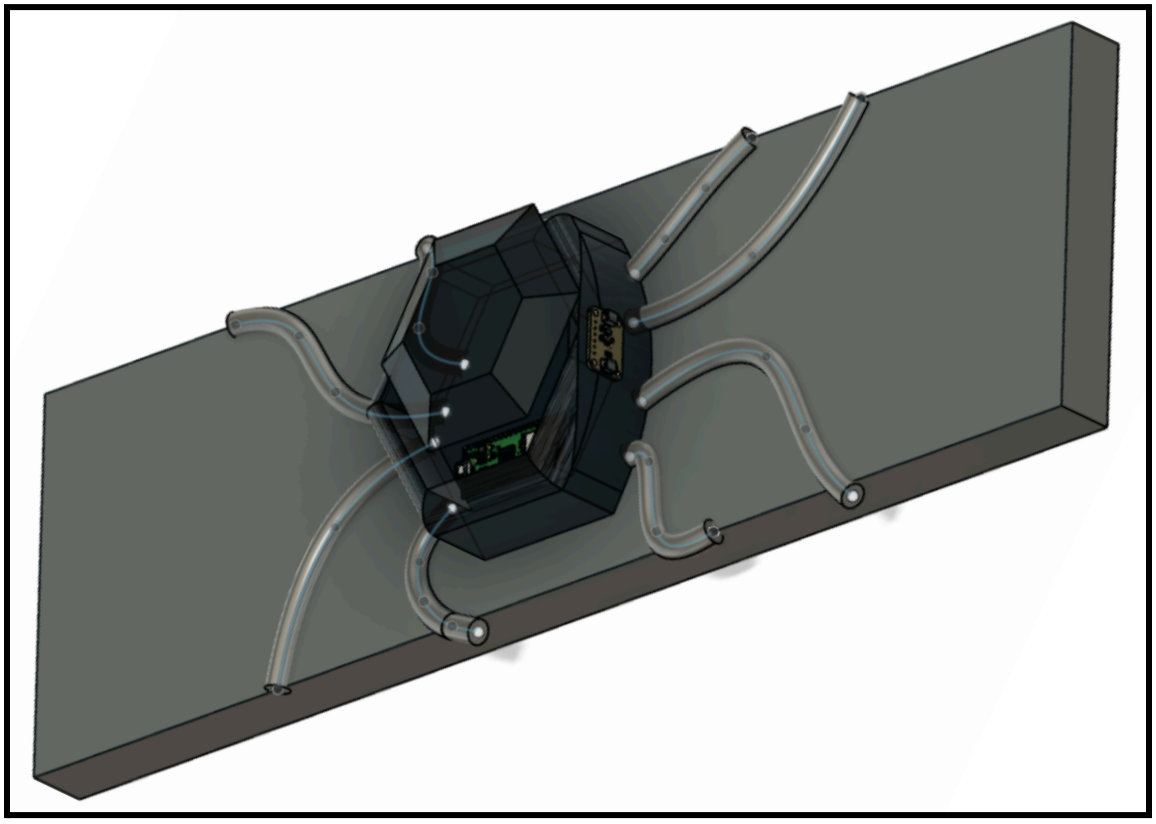

Table of Contents

Sensor Package for Internal Detection In Extraterrestrial Regions (SPIDER)

New Mexico Institute of Mining and Technology

HuLC HUMAN LANDER CHALLENGE

OBJECTIVE

Develop a wall-mounted sensor package to reduce weight and improve sensitivity of lunar base structural health monitoring systems

Technical Approach

- Design a prototype sensor housing node containing multiple sensing modalities
- Develop signal processing hardware and algorithms to identify critical structural or environmental damage
- Validate health monitoring capabilities through simulation and experimentation

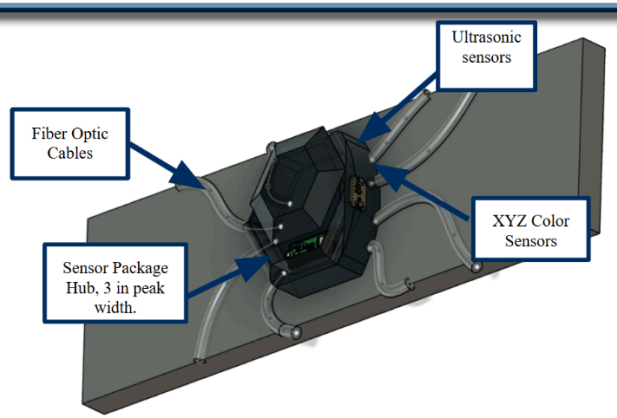

Fig 2: Prototype SPIDER Hub

Key Design Details & Innovations of the Concept

Innovation: reduced-size wall sensing nodes, cross-validated through 3 modalities to detect radiation, temperature, and structural damage

Bio-inspired design

Sensing design inspired by spider in a web

Ultrasonic

Sensing vibrations on thin wires across lunar wall substrate

Colorimetric paint

Radiochromic/thermochromic color sensing

FBGs

Web of dispersed optical cables

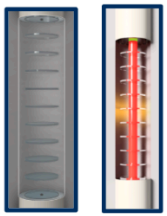

Fig 1: Fiber-Bragg Grating Sensor

	3/4/2026		NMIMT Human Lander Challenge		
Allocations					
	Source(s)	Amount			
1	HuLC Second Phase Funds	$ 9,000			
	Total Allocation:	$ 9,000			
Expenditures					
	Description	Budgeted	Spent to date	emaining to spen	Over/Under
1	Piezoelectrics	$1,200	$0	$1,200	$0
2	Fiber Optics	$1,200	$0	$1,200	$0
3	Colorimetric sensors	$1,200	$0	$1,200	$0
4	Hub assembly material	$1,200	$0	$1,200	$0
5	Contingency / Incidentals	$1,200	$0	$1,200	$0
6	Travel to forum	$3,000	$0	$3,000	$0
	Totals:	$9,000	$0	$9,000	$0
				Remainer of allocation	$0

Fig 3: Budget Calculations

Summer 2026, TRL 4: Conclusion of HuLC

↓

Year 0 of adoption, TRL 4-5: Lab environment system validation

↓

Year 1-2 of adoption, TRL 5-6: High-fidelity habitat analog testing

↓

Year 2-4 of adoption TRL 6-7: Operational environment demonstration

↓

Year 4-6 of adoption TRL 7-8: Qualification of final design

↓

Year 6-8 of adoption TRL 8-9: Success in lunar environment

1. Executive Summary

The Sensor Package for Internal Detection in Extraterrestrial Regions (SPIDER) is a distributed habitat-health monitoring node designed to reduce the mass, complexity, power, and maintenance burden associated with Environmental Control and Life Support System (ECLSS) health monitoring for 30-day lunar missions and future Mars missions. The sensor node combines fiber Bragg grating strain and temperature sensing, piezoelectric acoustic localization, colorimetric indication, local processing, and passive energy harvesting in a compact wall-mounted package.SPIDER will act as a node in a wired sensor network to diagnose and localize habitat anomalies and alert habitat crews. SPIDER is designed to reduce wiring needed for additional nodes and enable new sensing mechanisms not currently available for lunar habitat architecture. This paper summarizes SPIDER requirements, design trades, preliminary verification results, risk posture, and a path to flight within the HuLC 5–8 year horizon.

2. Operational Context & Problem Definition

Sustained lunar surface missions are expected to support crewed habitation for approximately 30 days, with long-term evolution toward extended lunar presence and Mars missions lasting up to 1200 days. In these missions, Environmental Control and Life Support Systems (ECLSS) are mission-critical infrastructure. Continuous awareness of temperature, humidity, pressure integrity, air quality, and structural condition is required to ensure crew survival. Unlike low Earth orbit operations, lunar and Martian habitats must function with limited resupply, constrained power budgets, reduced gravity, and restricted crew time for maintenance. Monitoring systems must therefore provide reliable health awareness without imposing excessive integration or operational burden. The NASA HULC presents the core challenge of the "Sensor Reduction in Hardware Health Monitoring Systems" as relating to the shortcomings of current sensor solutions. According to the challenge, current sensors are effective, but require much mass, complexity, and power usage. SPIDER is designed to directly address these problems with a robust inclusion of sensors in a light-weight and simple package, which is capable of harvesting its own power. SPIDER introduces no extra risk to crew, as it serves as a passive sensor system that works without intervention after installation, and features minimal barriers to adoption by NASA, as it is intended to affix to NASA's produced habitats. Although SPIDER sensor packages are intended for installation within the pressurized interior of a habitat, the broader exploration environment still drives design constraints. Systems must tolerate launch loads, long mission durations, vibration from rotating machinery, dust transported into the habitat, and radiation exposure. Over time, structural fatigue, small leaks, calibration drift, and gradual environmental shifts become more likely. Monitoring architectures must remain dependable and interpretable across these cumulative stressors.

Current space systems typically rely on distributed, powered point sensors that monitor hardware health using numerous temperature, pressure, humidity, and other dedicated sensing nodes. While effective, this approach scales through multiplication. Increasing monitoring confidence generally requires adding more sensors at more locations, which increases wiring, connectors, interfaces, and overall system complexity. Point sensors provide localized measurements, which can make anomaly localization difficult when issues develop between sensing nodes or propagate structurally. Many sensing channels also require continuous electrical power and periodic calibration, increasing baseline power demand and maintenance requirements. These characteristics create performance gaps for sustained lunar and Mars missions. Increasing sensor count to improve awareness can simultaneously increase integration burden, diagnostic ambiguity, and crew troubleshooting time. Limited spatial awareness can delay localization of developing leaks or structural anomalies. Continuous powered sensing reduces available operational margin in energy-constrained habitats. If these gaps are not addressed, future exploration missions risk higher

operational complexity and slower response to off-nominal events. Even when safety is preserved, ambiguous or poorly localized indications can consume crew time and reduce mission efficiency. As missions extend in duration and autonomy increases, monitoring architectures must provide clearer, more localized system awareness without proportional growth in sensor count and system complexity.

This defines the central challenge addressed by this proposal: improving ECLSS hardware and environmental health monitoring while reducing reliance on numerous discrete, powered point sensors and the architectural burden they impose.

3. SPIDER'S Sensor Subsystems

3.1. Passive Power Harvesting

To reduce wiring complexity and limit dependence on centralized habitat power, each SPIDER unit uses a combination of passive energy harvesting and onboard energy storage. The primary harvesting source is a photovoltaic cell mounted on the SPIDER housing to collect ambient interior lighting within the habitat. For preliminary analysis, the system assumes a conservative interior illumination level of approximately 300 lux. Under these lighting conditions, indoor-optimized photovoltaic cells can provide continuous trickle charging that offsets a portion of the node's operating load during normal mission conditions.

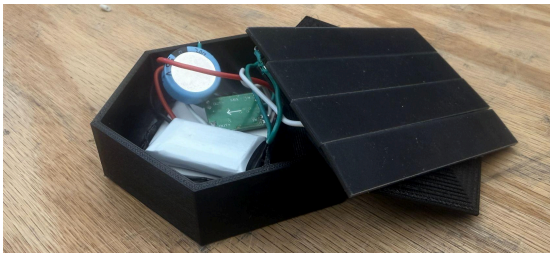

Figure 1: Power system including the photovoltaic cells, supper capacitor, Lipo battery, and the thermoelectric generator.

Each SPIDER unit includes a 1.67 Wh rechargeable battery to buffer harvested energy and maintain operation during periods of reduced lighting. In nominal monitoring mode, the unit samples sensors at 1 Hz to track structural vibration, environmental conditions, and system health indicators. Data is processed locally and periodically transmitted to the habitat monitoring computer through a prototype wireless communication link. Out-of-family measurements can trigger immediate alerts. In this mode, the estimated average power consumption is approximately 49.5 mW. If ambient lighting is unavailable, the battery alone can support approximately 34 hours of continuous nominal operation. When interior lighting is available, photovoltaic harvesting reduces the net battery drain and extends operational endurance.

If lighting is lost or the system is commanded into contingency operation, SPIDER transitions to an emergency low-power mode. In this mode, the microcontroller remains in deep sleep between measurements, and data is transmitted only when sensor readings exceed defined safety thresholds. A single daily health-status message confirms that the node remains functional. This reduces the estimated average power consumption to approximately 1.8 mW. With the onboard battery alone, emergency mode supports approximately 38 days of operation, exceeding the 30-day lunar surface mission target. Additional harvested energy can further extend this duration.

A thermoelectric generator (TEG) provides supplemental energy recovery when a thermal gradient exists between the electronics package and the monitored structural surface. Assuming a structural heat flux of 2

W/m² across a 50 cm² device footprint, approximately 10 mW of thermal power is available. With a conservative conversion efficiency of 2%, this corresponds to roughly 0.2 mW of electrical power. Although this contribution is small compared with nominal operating demand, it is useful during low-power contingency operation because it reduces net battery drain and can extend emergency monitoring endurance to approximately 40–45 days.

To improve resilience after complete battery depletion, each SPIDER unit also includes a supercapacitor energy buffer. In this recovery mode, the TEG gradually charges the capacitor until enough energy is available to briefly wake the microcontroller, sample the sensors, and check whether local conditions remain within safe limits. This allows SPIDER to perform periodic low-rate safety checks, estimated at approximately once every 10–15 minutes, as long as a usable thermal gradient remains across the monitored structure.

Together, photovoltaic harvesting, thermoelectric recovery, rechargeable storage, and supercapacitor buffering allow SPIDER to support long-duration monitoring while reducing the need for dedicated power wiring at every sensing location. The approach is not intended to make the system independent of all habitat power under every condition; instead, it reduces power infrastructure burden, extends battery life, and preserves limited monitoring capability during contingency scenarios.

3.2. Ultrasonic/Piezoelectric Sensor for Location Detections of Anomalies

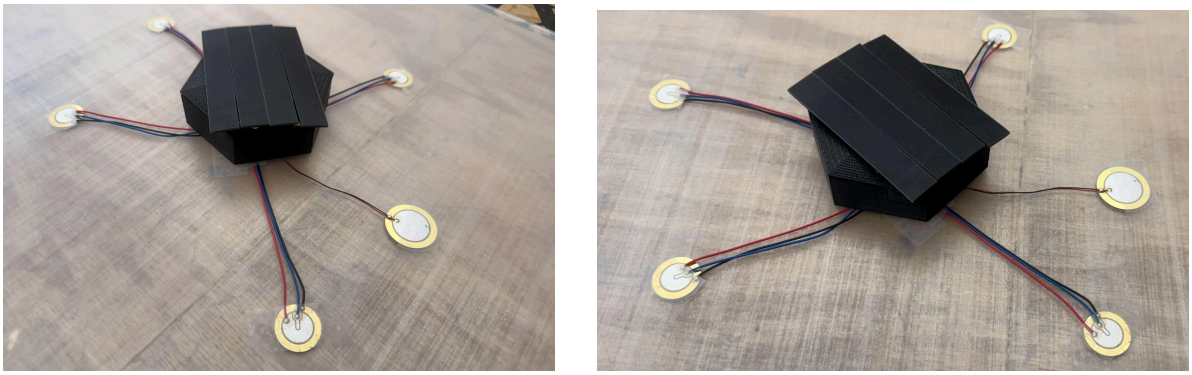

Figure 2: Testing setup with piezoelectric sensors installed on an acrylic sheet.

Structural and acoustic monitoring requires both detection of an abnormal event and estimation of where that event originated. In a lunar or Mars habitat, relevant events may include micrometeoroid-induced structural disturbances, small leak-like acoustic signatures, impacts, or abnormal vibration from nearby ECLSS hardware. Traditional point sensors can confirm that a disturbance occurred near a specific sensor, but they provide limited information when the event originates between sensors or propagates through the habitat structure.

SPIDER addresses this limitation using piezoelectric wafer active sensors mounted to the interior surface of the habitat wall or supporting structure. These sensors act as passive acoustic emission detectors. When a disturbance occurs, stress waves travel through the structure and are recorded by multiple sensors at slightly different times. By comparing the time difference of arrival between sensors, the SPIDER node can estimate the direction and approximate location of the event. Multiple SPIDER units can then operate as a larger distributed array, improving localization over a wider habitat region and allowing the system to distinguish between local disturbances, propagating structural events, and repeated vibration from nearby equipment.

Each piezoelectric channel includes signal amplification and high-pass filtering before the data are processed by the local controller. The amplifier increases the small voltage response generated by the piezoelectric element, while the high-pass filter reduces low-frequency background vibration from pumps, fans, crew movement, and other habitat operations. This signal conditioning improves the signal-to-noise ratio and reduces the likelihood of false alerts from normal mechanical activity.

The piezoelectric elements require no standby power at the sensing location because they generate a voltage response when mechanically excited. Subsystem power draw is therefore dominated by the signal-conditioning electronics, with the amplifier circuit estimated to draw approximately 0.05 mA during active operation. This low power requirement supports SPIDER's overall energy-minimization objective while still providing a useful pathway for detecting and localizing structural disturbances, leak-like acoustic events, and abnormal vibration signatures associated with habitat and ECLSS hardware.

3.3. Colorimetric Paint, XYZ Color Sensors, and Health-Centric Data Collection

In both lunar and terrestrial habitats, it is essential to monitor environmental changes that are not visible to the naked eye. For the SPIDER system, particular concerns include changes in air quality, ionizing radiation exposure, overheating of electronics, and the presence of aerosolized chemical compounds within human living spaces. To monitor these hazards, our approach draws on the principles of traditional colorimetric sensing. Colorimetric films, textiles, and dyes are a well-established area of research that rely on materials which react to specific substances of concern, producing fluorescence or visible color changes when exposure occurs.

SPIDER leverages this concept through the development of specialized colorimetric coatings. One approach involves a fluoride-based compound paint designed to detect radiation exposure, while additional nanochemical colorimetric dye paints are used to identify aerosolized chemical compounds in the surrounding air. To measure these changes, SPIDER incorporates an XYZ color sensor that detects shifts in the colorimetric coatings. These color changes serve as indicators of airborne hazards or radiation in the monitored environment. The sensor is embedded within the central hub of SPIDER and observes a dedicated strip coated with the colorimetric paints, although future implementations may involve applying the coatings directly to exposed structural surfaces. At this stage of development, a dedicated sensor strip provides greater experimental control. The strip will be mounted parallel to the floor of the testing environment to reduce dust accumulation, which is a significant concern in lunar environments. The XYZ color sensor will be mounted at a slight angle beneath a transparent protective shield within the SPIDER hub, allowing an unobstructed view of the inverted strip. An integrated LED illumination source will provide consistent lighting conditions to ensure accurate color detection. The strip itself remains exposed to the surrounding air, allowing the coatings to respond directly to gaseous hazards and airborne particulates.

Through this system, SPIDER aims to provide a simple and reliable method for monitoring environmental hazards that may affect human health in lunar habitats.

3.4. Fiber Bragg Grating Optical Sensors and Data Interpretation

Walls of a lunar base architecture will likely consist of composite structural and inflatable layers for environmental protection (Rojdev et. al, 2009). This type of structure requires constant, low power monitoring systems to identify damage and environmental changes that can be caused by the thermal cycling and radiation experienced on the lunar surface. Fiber Bragg Grating (FBG) optical cable offers a well-tested and flight-validated solution for constant lunar health monitoring. FBGs have a long history of use for structural health monitoring (SHM) in analogous environments, such as in composite structures in Alaskan winter (Xiao et. al, 2017). FBG sensors have been applied and tested in space environments as

well (Juwet et. al, 2024), proving sensor functionality in every application related to lunar base monitoring. FBG cables will provide a well-understood and tested baseline sensor to detect damage and structural abnormalities.

FBG cable sensors used in SHM can be dispersed over a large surface and can detect small changes in substrates. Bragg gratings have many benefits as a sensor in lunar structures, such as being resistant to electromagnetic interference and not requiring power or interrogation at the site of the sensor. For the SPIDER sensing project, this means that a single FBG interrogator can power an entire web of FBG optical sensors, which can be placed on any of the complex geometries that will be entailed in an internal lunar structure. Other sensing modalities within each node will allow for informed isolation of FBG signals for temperature or straining effects.

Fiber Bragg Gratings are formed by inducing a periodic modulation of the refractive index along the core of a single-mode optical fiber. This is usually accomplished through laser-produced partially reflective planes embedded within the optical fiber. The distance between reflective planes in the fiber is referred to as the grating pitch. An interrogator system induces light into the, and constructive interference occurs for light emissions at the same wavelength as the Bragg fiber pitch. Light emissions of the same wavelength as the Bragg pitch are reflected back toward the interrogator as a narrow spectral peak. On the opposite side of the grating, the optical spectra will have a missing peak at Bragg pitch. Both the reflected signal and the transmitted signal can be used for signal processing.

FBG sensing works by the changes in grating distance that occur when the cable experiences strain or other environmental changes. Axial strain stretches or compresses the Bragg pitch section of the cable, which will induce a phase shift in optical spectra data. Strain has additional effects on optical emissions, meaning a small change in surface stress can induce significant phase shift in FBG signals. Thermal expansion and temperature changes also affect optical transmissions, allowing for thermal anomaly detection through FBG sensing as well. Signal processing is usually accomplished through peak detection algorithms, such as cross-correlation or gaussian fitting. Arrays of FBGs along a single fiber with separate Bragg wavelengths allow simultaneous and distributed measurements of strain and temperature across an entire structure. Shifts in static strain fields can reveal load redistribution caused by crack initiation or delamination. Emissions from transient stress waves produced by crack propagation generate broadband signals that arrive at different FBG sensors with different time delays, which can allow damage localization.

4. Verification and Validation

4.1. Passive Power Harvesting

The passive power harvesting system was tested to evaluate whether SPIDER could reduce dependence on dedicated habitat power wiring while extending node operation during reduced-power conditions. The system combined indoor photovoltaic harvesting, thermoelectric recovery, a rechargeable battery, and a supercapacitor energy buffer. The purpose of this verification test was to determine whether these components could support nominal monitoring, extend emergency monitoring, and allow limited recovery operation after low-energy conditions.

Acquisition of Materials
The test used commercially available indoor photovoltaic cells, a thermoelectric generator, a 1.67 Wh rechargeable battery, a supercapacitor, and representative low-power SPIDER electronics. Off-the-shelf components were selected so testing could focus on power balance, charging behavior, and operating duration rather than custom energy-harvesting hardware development.

Test Bed Set-Up
The photovoltaic cell was mounted on a SPIDER-like housing and exposed to controlled indoor lighting, with testing centered around approximately 300–500 lux. The thermoelectric generator was mounted between the SPIDER package and a representative structural surface, where a controlled temperature difference was applied. The node was tested in nominal mode, emergency low-power mode, and recovery mode.

Data Acquisition
Testing recorded harvested voltage, harvested current, battery voltage, supercapacitor voltage, node current draw, and total runtime. Photovoltaic testing measured charging contribution under controlled lighting. Thermoelectric testing measured generated power under a controlled temperature gradient. Battery testing compared runtime in nominal and emergency modes. Recovery testing determined whether the supercapacitor could store enough harvested energy to wake the system and complete a short sensor check.

Results
The collected data demonstrated that both photovoltaic and thermoelectric harvesting produced measurable charging contributions under representative test conditions. The rechargeable battery supported the expected operating modes, and emergency low-power operation substantially extended node endurance compared with nominal monitoring. The supercapacitor recovery test also demonstrated that harvested energy could be buffered long enough to support a brief wake cycle and sensor check after low-energy conditions.

Table 1: Power produced by the photovoltaic cells and thermoelectric generator.

Power Generator	Voltage	Current	Key Takeaways
Photovoltaic cell (at a light level of 300 lux)	8.41v	51.6mA	Produced the strongest power contribution.
Thermoelectric Generator	0.45v	2.21mA	Very small power contribution

Success Criteria
The passive power harvesting test was considered successful because the photovoltaic cell produced measurable charging contributions however the thermoelectric generator did not contribute nearly as much energy as calculated. The battery supported both nominal and emergency operating modes, and the supercapacitor provided enough stored energy for a brief recovery-mode sensor check. Overall, the test demonstrated that passive harvesting and onboard storage can reduce reliance on dedicated power wiring and preserve limited monitoring capability during contingency operation.

4.2. Ultrasonic/Piezoelectric Sensors

The piezoelectric sensing subsystem was tested to evaluate whether SPIDER could detect and localize structural or acoustic disturbances on a representative habitat surface. The subsystem used commercially available piezoelectric sensors mounted to a flat structural panel at known locations. Controlled impacts were applied at marked test points to simulate structural disturbances, while the sensor outputs were recorded to compare signal arrival times across the array.

The localization method was based on the time difference of arrival between sensors. For a disturbance at an unknown location (x,y), the distance to sensor iii, located at (x_i, y_i), was modeled as

$$d_i = \sqrt{(x - x_i)^2 + (y - y_i)^2}$$

The arrival-time difference between sensors i and j was then estimated using

$$\Delta t_{ij} = t_i - t_j = \frac{d_i - d_j}{c}$$

where c is the wave speed through the test panel. This approach allowed the system to estimate the source location without requiring the exact start time of the impact.

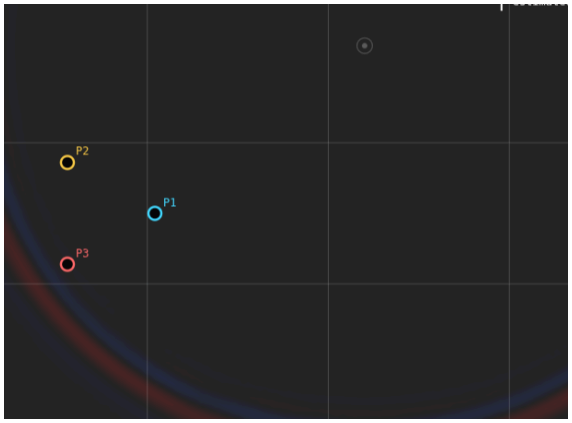

Figure 3: Si

Before physical testing, wave propagation was simulated in code to refine the localization method. The simulation modeled stress waves traveling across a rectangular panel, including wave arrival at multiple virtual sensor locations and reflected waves from panel boundaries. This allowed sensor placement, timing logic, and localization calculations to be adjusted before applying the method to physical test data.

During validation testing, each trial recorded the known impact location, sensor response, arrival-time differences, estimated event location, and localization error. Localization accuracy was evaluated using

$$e = \sqrt{(x_{\text{est}} - x_{\text{true}})^2 + (y_{\text{est}} - y_{\text{true}})^2}$$

where (x_{cst}, y_{cst}) is the estimated location and (x_{true}, y_{true}) is the known impact location.

Results

Table 2: Localization data of the piezoelectric sensors.

Test Case	Impact Energy / Input	Nearest Sensor Distance	Farthest Sensor Distance	Detection Rate	Avg. Localization Error	Max Error	Key Takeaway

Low energy impact	0.05 J	75 mm	425 mm	90%	24 mm	34 mm	Low-energy events were detectable but had the highest error
Medium energy impact	0.15 J	75 mm	425 mm	100%	17 mm	26 mm	Best balance of clear signal and repeatable localization
High energy impact	0.30 J	75 mm	425 mm	100%	13 mm	21 mm	Strong signals improved timing accuracy and localization
Near sensor impact	0.15 J	50 mm	390 mm	100%	14 mm	22 mm	Events near one sensor were detected clearly
Center panel impact	0.15 J	210 mm	310 mm	100%	16 mm	24 mm	Central impacts produced consistent arrival-time differences
Edge region impact	0.15 J	85 mm	460 mm	95%	23 mm	32 mm	Edge effects and reflections slightly increased error

The test was considered successful because the piezoelectric array consistently detected controlled impact events, recorded measurable timing differences between sensors, and produced repeatable location estimates. The simulation and physical test results together supported the use of piezoelectric sensing as a low-power method for detecting and localizing structural or acoustic anomalies within the SPIDER architecture.

4.3. Colorimetric Hazard Sensing

The colorimetric sensing component of SPIDER has many envisioned modes of hazard detection through the various dyes employed on the strip, each used for a distinct hazard mode. Though the envisioned final product of SPIDER is planned to have dyes/paints capable of detecting ionizing radiation, excess CO2, and more, it was determined that calibration/validation of the testing sensor was to be prioritized. As such, it was deemed to be essential to study an easily replicated hazard first and foremost. This hazard was chosen to be temperature sensing. Temperature monitoring of interior habitat walls is a critical method of hazard detection. The walls of habitats serve as crucial barriers between the harsh lunar environment and those working within the habitat. During a Lunar day, the moon can reach temperatures higher than 250 ℉ (NASA, *"Weather On The Moon")*. Lunar environments, while insulated, are likely to be susceptible to heat hazards, which would damage electronics and contribute to hazards for humans. Even though temperature sensing is used for its practicality in testing, it is also a key hazard to be monitored. As such, the following test plan was produced:

Acquisition of Materials

The colorimetric test will use commercially available heat-reactive paint with a known transition temperature. Using an off-the-shelf coating reduces uncertainty associated with custom paint formulation and allows the test to focus on the sensor readout, illumination control, threshold detection, and alert response. An off-the-shelf XYZ color sensing module will be used to measure the coating response. A simple LED or buzzer alert will be included as an external verification output so that successful detection can be confirmed without relying only on logged data.

Test Bed Set-Up

The test bed will use a SPIDER-like geometry with a controlled LED illumination source directed toward a coated test strip. Fixed illumination removes room-light variability and provides a repeatable optical baseline for color measurements. Heat-reactive paint will be applied to a dedicated test strip positioned within the sensor field of view. The strip angle and sensor distance will remain fixed throughout testing to isolate the effect of temperature-driven color change.

Data acquisition

The test strip will be exposed to controlled temperature steps beginning near ambient conditions and increasing through the paint transition temperature. At each step, alert state and time response will be recorded. Testing will record the temperature at which the alert threshold, as well as the sensitivity needed. The heating element will be brought to the target temperature before exposure to the strip so that the color-change response can be evaluated under controlled and repeatable conditions.

Success Criteria

A successful colorimetric test will demonstrate a repeatable sensor response to a controlled temperature-driven color shift. Initial testing will focus on the lower end of the heat-hazard range to avoid unnecessary heating while still demonstrating threshold detection relevant to electronics and wall-component monitoring. Success will be defined as consistent detection of the color transition under fixed illumination, activation of the alert output at the selected threshold, and no false alert during baseline ambient trials.

A testbed was created to simulate conditions similar to those found in the interior of a lunar habitat, as well as simulating the structure in integrated SPIDER. The color sensor was mounted into a housing that ensured light controllability while also allowing air exposure to the thermoreactive paint. An LED was used as the main source of the colorimetric sensor's lighting, but ambient light was present, as would be expected in a lunar habitat. Additionally, the thermal paint was mounted parallel with respect to the floor, to simulate the dust-tolerant design required. The sensor, however, was not mounted at an angle as would be ideal for the dust tolerance, as angle of the sensor was a variable undesirable to testing at this time.

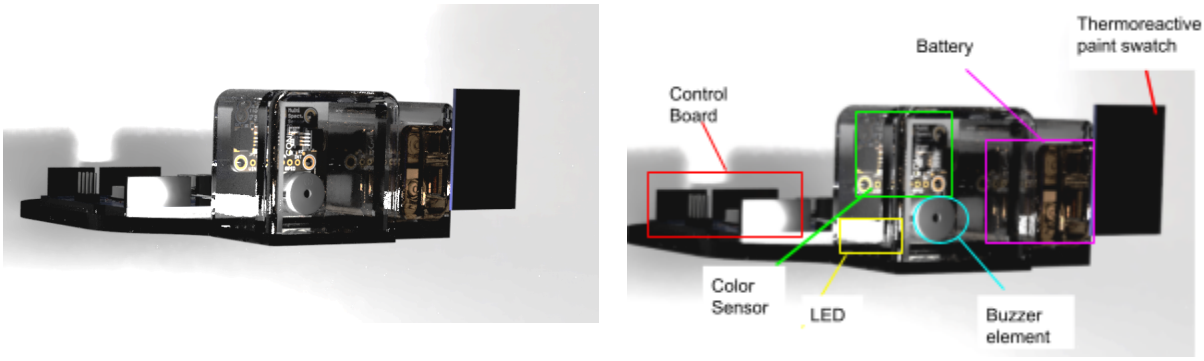

Figure 4: rendering of testbed (left) and description of testbed (right)

To control for the detection of colors and ensure that a color shift could be measured satisfactorily, the colorimetric sensor was coded to account for many different factors. The AS7341 sensor, our sensor of choice, is implemented as an eight-channel spectral color sensor rather than a conventional RGB sensor. The sensor measures reflected light intensity across eight discrete wavelength bands: 415 nm, 445 nm, 480 nm, 515 nm, 555 nm, 590 nm, 630 nm, and 680 nm. Together, these channels provide a spectral image of the test surface, allowing changes in the paper or coating color to be detected with greater

specificity than a three-channel RGB measurement. During initialization, the system acquires 50 consecutive spectral readings from the test surface. Each reading contains intensity values from all eight wavelength channels. These readings are averaged to establish an initial baseline, which represents the starting color condition of the paper. With a 100 ms delay between samples, this baseline acquisition process requires approximately 5 seconds, with minor additional time associated with sensor readout. Before comparison, each spectral reading is normalized by dividing the value of each channel by the total measured signal across all eight channels. This is illustrated with the equation below:

$$\text{Normalized Channel}_i = \text{Channel}_i / (F1 + F2 + F3 + F4 + F5 + F6 + F7 + F8)$$

Channel_i is the measured intensity of a specific AS7341 wavelength channel, and F1 through F8 are the measured intensities at 415 nm, 445 nm, 480 nm, 515 nm, 555 nm, 590 nm, 630 nm, and 680 nm, respectively. This normalization process reduces sensitivity to changes in overall illumination intensity and emphasizes relative spectral distribution. As a result, uniform brightness changes, such as a slight increase in LED output, have less influence on the detection result than true changes in reflected color. After the baseline has been established, the system acquires a new spectral reading every 250 ms, corresponding to a sampling rate of approximately 4 Hz. Each new reading is normalized using the same method as the baseline. The normalized current reading is then compared against the normalized baseline by calculating the absolute shift in each of the eight wavelength channels and summing these shifts into a single total difference value. A detection threshold of 0.035 was selected as the sensitivity criterion for identifying color changes in the thermochromic paint. When the total normalized spectral shift exceeds 0.035, corresponding to approximately a 3.5% cumulative spectral change across the measured channels, the system classifies the surface as having changed color and activates the buzzer. If the difference remains below 0.035, the surface is treated as unchanged and the buzzer remains inactive. To account for gradual lighting variation and sensor drift, the baseline is updated only when no color change is detected. This update is performed using a slow adaptation factor of 0.005. Under this condition, each normal reading contributes 0.5% to the updated baseline, while the previous baseline contributes 99.5%. This allows the system to compensate for slow environmental drift without rapidly adapting to an actual color-change event. When the spectral difference exceeds the detection threshold, baseline updating is suspended and the passive buzzer is driven with a 2000 Hz tone to indicate detection.

From the manufacturer, the paint is a stable hue at a minimum temperature of 18℃ or roughly 65℉ (or just about room temp). Manufacturer instructions also show that from 30℃, or 33℃ (86℉ and 91.4℉) there is an obvious shift. Experimentally, a most distinct and reliable visual color shift was found to be at the lowest temperature of 30℃, as such, we established a "threshold temperature" for our first experiment to be 30℃. This can be reasonably assumed to mimic the conditions of critical electronic systems in the wall just beginning to radiate or conduct heat to the sensor. Data is organized in Table 2 to determine the sensitivity needed for the sensor.

Table 3: Threshold Sensitivity Comparison for Colorimetric Detection Results

Parameter	0.100	0.090	0.080	0.070	0.060	0.050	0.040	0.035	0.030	0.020	0.010
Sensitivity	Very low	Very low	Low	Low	Mod. low	Moderate	High	**High**	Very high	Extremely high	Maximum
Recognition Time	None	None	None	None	None	None	Variable	**~0.25 s**	~0.25 s	~0.25 s	~0.25 s
Detection Success	0%	0%	0%	0%	0%	0%	50–75%	**100%**	100%	100%	100%
Interpretation	Too high	Too high	Too high	Too high	Too high	Misses change	Inconsistent	**Selected threshold**	Noise sensitive	Very noise sensitive	Least robust

A sensitivity of 0.035 was determined to be the most ideal for our purposes; not too sensitive, and not too insensitive. Now that our sensitivity is established, we test for how long it takes for a temperature change to be detected, at low and high critical temperatures, it is common knowledge that most electronics will just be beginning to experience difficulties around 30-35 ℃. As early hazard detection is critical, we measure for temperature shifts at this low end of malfunction temps, and end at 40 ℃, when the data appears to show 100% reliability. Reliability, in this case, is a subjective measurement of the quality of the response in relation to the observable color change in the paint. Results of this testing are detailed in Table 3.

Table 4: Temperature Dependent Colorimetric Detection Response Results

Parameter	30 °C	31 °C	32 °C	33 °C	34 °C	35 °C	36 °C	37 °C	38 °C	39 °C	40 °C
Hazard Level	Early warning	Early warning	Early warning	Low critical	Low critical	Low critical	Moderate	Moderate	High	High	**Upper critical**
Detection Time	~9.5 s	~8.0 s	~7.5 s	~5.5 s	~4.5 s	~3.5 s	~3.0 s	~2.0 s	~1.5 s	~1.0 s	**~0.5 s**
Detection Reliability	Low	Low	Moderate	Moderate	High	High	High	Very high	Very high	Near 100%	**100%**
Practical Interpretation	Earliest possible warning	Weak color response	Developing shift	Low-end malfunction range	More visible shift	Common warning point	Clear transition	Strong transition	Fast response	Nearly reliable	**Fully reliable**

The testing demonstrates that the sensor is easily tuned for ideal hazard detection, as well as the success of the ‘baseline establishment and comparing’ method of data collection and alerting. This sensor would be capable of detecting early thermal hazards in a lunar habitat.

4.4. Fiber Bragg Grating Optical Sensors

The Fiber Bragg Grating (FBG) sensors are to be distributed across the SPIDER habitation wall network, and are interrogated using a single laser source. The cable will be used to record reflected spectra, analyzed at the interrogator to extract strain, temperature, or vibration measurements at each grating node. The FBG sensors require no local power, so the single interrogator can service an entire cable run as long as each FBG comb on a shared cable is of a distinct wavelength band. To enable anomaly detection, each FBG sensor must be calibrated to map reflected wavelength shifts to mechanical strain. The following experiments establish this calibration so the FBGs can be used for strain and temperature measurements.

Experiment setup

A cantilevered beam setup was used to calibrate strain readings from the fiber bragg grating cable. A Luna Innovations OS1100 Optical cable was used, with one FBG placed at the same location on the beam as a strain gauge. The strain gauge was a Micro-Measurements Linear strain sensor, and was calibrated previously. Both sensors were attached using Hysol Epoxy. Displacement was applied to the free end of the beam using a loading micrometer. Readings were taken using NI-instruments strain modules with a NI-DAQ and labview, and results were exported to CSV to be read in python/matlab.

A cantilevered beam configuration was used to calibrate FBG strain readings against a reference strain gauge. A Luna Innovations OS1100 optical fiber was used, with one FBG placed on the beam at the same location as a pre-calibrated Micro-Measurements linear strain gauge. Both sensors were bonded to the beam surface using Hysol space-grade epoxy after surface treatment. Displacement was applied to the free end of the beam using a loading micrometer. Data acquisition was performed using National Instruments strain modules with a NI-DAQ system and LabVIEW, and results were exported to CSV for post-processing in Python and MATLAB.

Figure 5: Experimental setup for FBG calibration, showing strain gauge and FBG sensor placement at the same location on a cantilevered beam deflected at its free end.

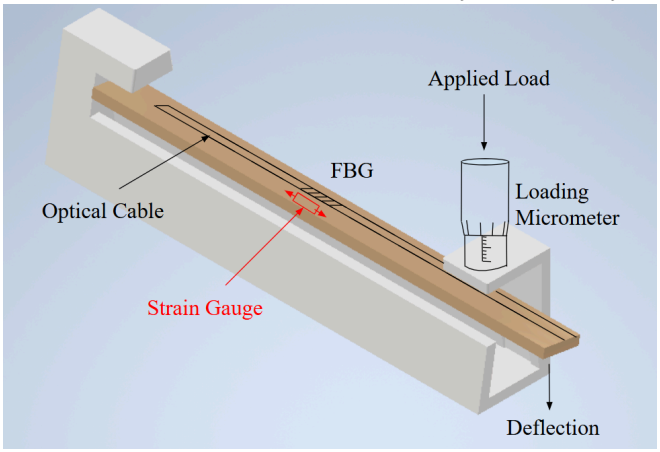

Spectra readings and peak detection

FBG readings were acquired as reflected spectra. Shifts in the Bragg grating period produce light spectra changes in the peak reflected wavelength. The value of this reflected wavelength can be extracted using a simple peak finding algorithm in Python, or even more simply through finding the max value in the data. With no load applied, the zero-load Bragg wavelength was measured at 1579.8 nm with both methods, very close to the manufacturer specification of 1580 nm grating.

Figure 6: FBG sensors reflect a certain wavelength of light back to the laser interrogator. The input laser includes a large band of wavelengths, while the reflected spectra is typically a narrow gaussian peak centered around the sensor grating wavelength. Shifts in reflected wavelength are used for measurements.

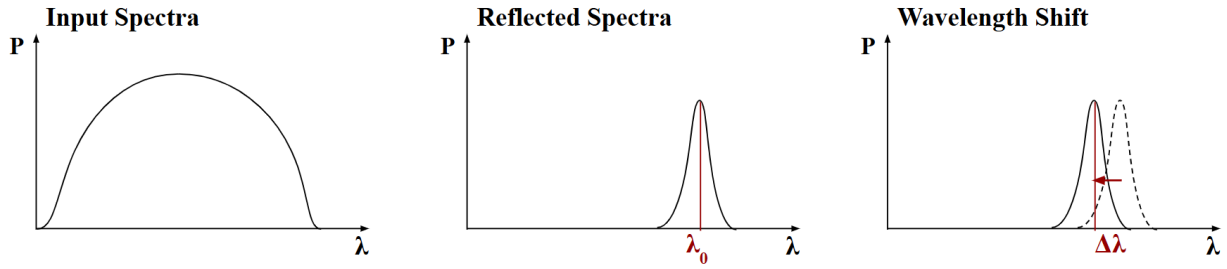

Strain constant formulation

In order to convert FBG spectra readings to strain, we used the following strain measurement formulations provided by [Source] for FBG cables.

$$\frac{\Delta\lambda}{\lambda_0} = k \cdot \epsilon_m + k \cdot \alpha \cdot \Delta T$$

where $\Delta\lambda/\lambda_0$ is the normalized wavelength shift (analogous to mechanical strain), k is the gauge factor relating wavelength shift to strain, αs is the substrate thermal expansion coefficient, and ΔT is the temperature change at the sensor. It is worth noting that temperature has additional effects on light spectra and FBG readings further than just mechanical strain, but this equation assumes only strain effects, which is sufficient for FBG calibration [].

For initial calibration in a room with constant temperature conditions, the thermal term was neglected, yielding a linear relationship between wavelength strain and mechanical strain:

$$\epsilon_m = k \cdot \frac{\Delta\lambda}{\lambda_0} + \epsilon_0$$

Here, we can find k and epsilon 0 values to minimize error between the wavelength strain and strain gauge measurements ϵ_m. The calibration constants k and ε_0 were determined by minimizing mean squared error.

$$MSE = \frac{1}{n}\Sigma_{i=1}^{n}(y_i - (k \cdot x_i + \epsilon_0)$$

The mean squared error can be minimized between FBG-derived and strain gauge measurements using gradient descent on the following cost function:

$$\hat{y} = \theta_0 + \theta_1 x$$

$$J(\theta_0, \theta_1) = \frac{1}{2m}\Sigma_{i=1}^{m}(\theta_0 + \theta_1 \cdot x_i - y_i)^2$$

Here, m is the number of iterations used in a gradient descent, optimizing using a cost function J. Training rate can be incorporated to calculate theta values using parameter updates:

$$\theta_0 := \theta_0 - \alpha\frac{1}{m}\Sigma_{i=1}^{m}(\hat{y}_i - y_i)$$

$$\theta_1 := \theta_1 - \alpha \frac{1}{m} \Sigma_{i=1}^{m} (\hat{y}_i - y_i) x_i$$

Here, alpha is the training rate. However, using a single training rate value for the x and y parameters is problematic for training time when the x parameters (wavelength strain) has a small-valued variance. In order to compensate for this, the wavelength strain was normalized using z-score (median and standard deviation) to allow for faster training time. After optimization, the optimal linear regression parameters can be extracted using the following de-normalized equations:

$$\theta_1 = \frac{\overline{\theta_1}}{\sigma}$$

$$\theta_0 = \theta_0 - \frac{\mu \cdot \overline{\theta_1}}{\sigma}$$

where μ and σ are the mean and standard deviation of the wavelength strain input, and barred θ values denote normalized regression parameters.

Results

Three independent test runs were conducted, each yielding consistent linear regression performance as shown in Figure 7. Calibration metrics are summarized in Table 4.

Figure 7: Three different test runs of strain data compare FBG wavelength readings to strain gauge readings, with consistent linear regression metrics.

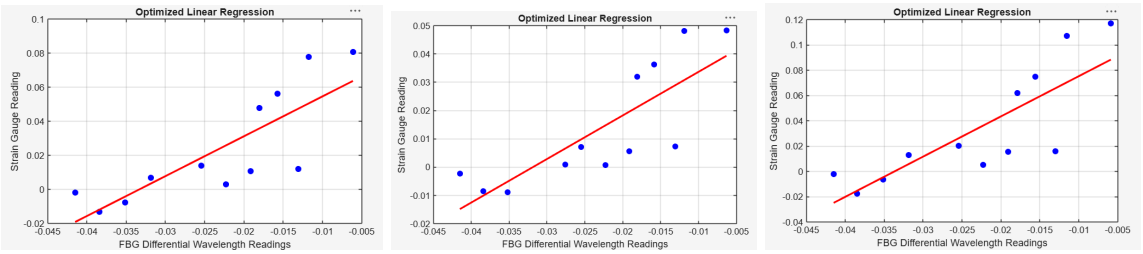

Table 5: Average mean square error and linear regression parameters after three test trials

Trial Number	1	2	3	Average
Mean Squared Error	0.0003	0.0001	0.0006	0.0004
Theta0 (Strain)	0.0780	0.0491	0.1072	0.0781
Theta1 (k)	2.3418	1.5410	3.1805	2.3544

The theta 1 value can be used as the k value comparing wavelength strain to mechanical strain, which was averaged to 2.3544 mechanical strain per wavelength strain. With this value, total mechanical strain can be measured at each FBG sensor, and temperature measurements can also be taken, based on the application of the FBG sensor. This calibration allows these sensors to calculate true mechanical strain using the following equation, when material thermal expansion coefficients are known:

$$\varepsilon_m = \frac{1}{k} * \left(\frac{\Delta\lambda_m}{\lambda_{0m}} - \frac{\Delta\lambda_T}{\Delta\lambda_{0T}} * \left(\frac{k * \alpha_{sp} + \alpha_\delta}{k * \alpha_{glass} + \alpha_\delta}\right)\right)$$

5. Mission Readiness

5.1 TRL Analysis and Schedule

When evaluated against NASA's Technology Readiness Level (TRL) framework, SPIDER currently falls below the maturity required for mission deployment. Our project presently stands at TRL 4, where components have been validated in a laboratory environment. Technology intended for operational space missions must typically reach TRL 9, indicating full system validation in a flight-proven environment. In order to bring SPIDER to this level, we must continue to perform extensive validation and iterate on the design. Because SPIDER is designed to monitor environmental hazards that directly affect human safety, extensive validation is not only necessary to follow the TRL path, but also to ensure that many potential modes of failure are addressed.

In the Human Lander Proposal paper, the team had the goal of advancing the sensor to a TRL 4, a goal that has been met. As such, we have revised the scope of our mission readiness timeline. This timeline outlines the major milestones required to mature the technology from early-stage experimentation to a validated prototype system. A detailed timeline of team objectives during HuLC development is shown in Appendix 4. As of the conclusion of the HuLC competition, the SPIDER system has reached TRL 4, where individual components and subsystems have been validated in a laboratory environment. To progress toward mission implementation within the next 5–8 years, a structured technology maturation timeline has been developed. This roadmap outlines the steps required to advance SPIDER through progressively more realistic testing environments, including habitat analog demonstrations, environmental qualification, and ultimately flight demonstration. Each phase focuses on increasing system integration, reliability, and environmental validation to meet the standards required for human spaceflight hardware.

Table 6: mission ready scope timeline

Phase	Year	TRL	Goal	Key Activities	Exit Criteria
Post-HuLC Baseline	0	TRL 4	Component and subsystem validation in lab environment	Integrated prototype from HuLC competition; initial sensor calibration; baseline hazard detection demonstrations	Documented lab validation of integrated SPIDER prototype
Phase 1 – Environment Validation	0–1	TRL 4 → TRL 5	Validate integrated system in habitat-like environment	Build Gen-2 prototype; of color, ultrasonic, and fiber optic sensors; conduct testing and hazard simulations	Repeatable detection of hazards in relevant environment testing
Phase 2 – Prototype Demonstration	1–2	TRL 5 → TRL 6	Demonstrate prototype in high-fidelity habitat analog	Build Gen-3 prototype; integrate with habitat systems simulators; run long-duration tests; evaluate reliability	Documented system performance in habitat analog testing

Phase 3 – Operational Prototype	2–4	TRL 6 → TRL 7	Deployment-like system demonstrated in operational environment	Develop environment-like hardware; EMI/EMC testing; vibration and handling testing; dust ingress tests; integrate with habitat engineering test unit	Operational demonstration and verification reports
Phase 4 – Qualification	4–6	TRL 7 → TRL 8	Qualification of final design	Build qualification and flight units; thermal-vacuum testing; vibration and shock testing; finalize firmware and interfaces	Completion of qualification test campaign and readiness reviews
Phase 5 – Full implementation	6–8	TRL 8 → TRL 9	Demonstrate system in space environment	Deploy SPIDER in lunar habitat module; monitor environmental hazards during mission	Successful mission operation and performance verification

5.2 Development, Verification, and Validation risks with mitigation strategies

To ensure the SPIDER sensor package performs reliably, the system will undergo multiple cycles of verification and validation testing focused on its core performance parameters: hazard detection sensitivity, response time, sensor reliability, and multi-system integration. Because SPIDER is intended to operate within a climate-controlled lunar habitat environment, ground testing will primarily be conducted in air-conditioned, earth-atmospheric, laboratory conditions. Following further subsystem validation, integrated testing will be conducted, where all three sensing systems operate simultaneously to verify coordinated hazard identification and system reliability. System acceptance will be determined by successful detection of test hazards within defined sensitivity and response thresholds while maintaining stable sensor output during continuous operation. Key risks include sensor integration complexity, detection sensitivity limitations, and schedule constraints associated with prototype fabrication. These risks will be mitigated through modular subsystem testing, early integration trials, and iterative prototype refinement throughout the development timeline. A detailed list of risks and a comprehensive risk matrix are shown in Appendix 3.

5.3 Project Cost

The project budget is split into two separate tracks: the immediate competition budget and the larger mission-readiness cost estimate. The budget presented in Appendix 2, “Budget 1”, presents the $9,000 competition scope budget, funded through HuLC second-phase funds, and allocates the available money across the main prototype development needs. The largest competition expense is travel to the forum at $3,000, while the remaining $6,000 is evenly distributed across piezoelectrics, fiber optics, colorimetric sensors, hub assembly materials, and contingency/incidental expenses. This shows that the competition budget is focused on building and demonstrating a functional bench-scale prototype rather than fully qualifying the system for spaceflight. The second and third budgets found in Appendix 2 as “Budget 2” expand the budget into a mission-readiness scope estimate using a work breakdown structure. The WBS table identifies the major phases required to mature the system, including concept development, detailed design, sensor fabrication, operational prototype testing, qualification testing, bench-level testing, flight demonstration, mission operations, and program management. Each cost item is tied to a cost driver and source factor, such as university labor rates, vendor quotes, NASA facility testing, rideshare references, and program management overhead. The final mission-readiness estimate totals approximately $4.081 million, with the largest projected costs coming from flight demonstration, qualification testing, bench-level testing, and operational prototype testing. Together, these graphics show that the current

$9,000 budget supports early prototype validation, while the larger WBS-based estimate represents the additional funding required to mature SPIDER toward a flight-relevant system.

6. Conclusion

Future manned missions to the moon and beyond will require robust ELCSS to ensure inhabitants of lunar bases are safe from extraterrestrial environments. The current trajectory of lunar habitat life support infrastructure involves power hungry and high-mass sensor environmental sensor systems that may not be feasible in missions with tight margins. Current proposed environmental monitoring solutions use sealed wireless node packages that scale well, but are power and mass hungry. In this paper, we expand the work done on colorimetric, piezoelectric array, and FBG sensing to enable new methodologies for environmental monitoring. These approaches could also enable sensing for complex lunar base geometry, and could function in electromagnetically harsh environments. Our work aims to enable ECLSS monitoring systems that can detect and localize habitat anomalies for the next generation of manned space missions.

7. Appendices

Appendix 1: TRL Chart

Technology	2026	2027	2028	2029	2030	2031	2032
Fiber Bragg Gratings	8	9	9	9	9	9	9
Piezoelectric Wafers	5	6	6	7	7	8	8
Colorimetric Sensors	3	3	5	5	6	6	7
Raspberry Pi-Pico	8	8	8	9	9	9	9

TLR Chart 1: Predicted readiness of each utilized technology for in-space application

Appendix 2 : Budgets

	3/4/2026		NMIMT Human Lander Challenge		
Allocations					
	Source(s)	Amount			
1	HulC Second Phase Funds	$ 9,000			
	Total Allocation:	$ 9,000			
Expenditures					
	Description	Budgeted	Spent to date	emaining to spen	Over/Under
1	Piezoelectrics	$1,200	$0	$1,200	$0
2	Fiber Optics	$1,200	$0	$1,200	$0
3	Colorimetric sensors	$1,200	$0	$1,200	$0
4	Hub assembly material	$1,200	$0	$1,200	$0
5	Contingency / Incidentals	$1,200	$0	$1,200	$0
6	Travel to forum	$3,000	$0	$3,000	$0
	Totals:	$9,000	$0	$9,000	$0
				Remainer of allocation	$0

Budget 1: competition scope budget

WBS	Description	Cost Driver	Source Factor
1.1	Concept & Requirements(Phase 1)	1.5 staff-months; $9,000 FTE-Yr (undergrad @ $6k/mo equivalent)	NAFCOM "Advanced Structures"; university stipend rate
1.2	Preliminary & Detailed Design (Phase 1 & 2)	4 staff-months + CAD/FEM licenses (~$500 student licenses)	NAFCOM multiplier 1.15x labor; student edition software pricing
1.3	Prototype & Sensor Fabrication (Phase 2)	FBG sensors x6, PWAS x10, colorimetric films x20, PCBs, Raspberry Pi Pico, other sensors	Vendor quotes: FBG ~$150/ea, PWAS ~$30/ea, Pico ~$5/ea, PCB ~$200 batch
1.4	Operational Prototype Testing (Phase 3)	EMI, EMC, Vibration testing	NASA SBIR Program
1.5	Qualification (Phase 4)	Thermal and shock testing at NASA facility	NASA CCRPP
1.6	Sub-scale & Bench-level Tests (Phase 4)	Lab bench time ~80 hrs, vibration fixture rental, data acquisition system	University lab rate ~$25/hr; DAQ rental ~$500; GSFC-STD-7000 ref.
1.7	Flight Demo (Phase 5)	Rideshare Costs	ISS CLD rideshare ICD reference
1.8	Mission Ops & Data Analysis	data review, 2 undergrad analysts	undergrad labor ~$20/hr x 200 hrs

WBS	Description	Cost Driver	Source Factor
1.9	Program Mgmt., QA, Systems Eng.	15% addition on WBS 1.1–1.6	NASA norm; advisor oversight included

WBS	Costs ($1000s)
1.1	9
1.2	25
1.3	2
1.4	200
1.5	400
1.6	300
1.7	3000
1.8	5
1.9	140
Total	4081

Budget 2: Mission readiness scope budget

All costs are preliminary placeholders based on NAFCOM parametric estimates, published vendor quotes, and standard university labor rates

Appendix 3: Risk matrix

Table 4: Risk evaluation matrix

Likelihood	5					
	4					
	3		6	3, 4		
	2					1
	1				2, 5	
		1	2	3	4	5
		Consequence				

Table 5: Description of identified risks

No.	Risk	Description	Mitigation
1	Sensor failure during deployment	Sensors may be damaged or improperly installed, preventing them from providing health monitoring data and potentially allowing damage to go undetected.	Prioritize ease of packaging and installation to reduce the chance of deployment errors.
2	Detection sensitivity limits	The sensor network may be installed successfully but still fail to detect critical health indicators within the system.	Use three complementary sensor modalities and perform testing in relevant environments to validate detection capability.
3	Design is too heavy	The sensor system may exceed mass limits, reducing the benefit of replacing existing methods.	Continuously optimize the design to minimize weight throughout development.
4	Design uses too much power	Excessive power consumption may be impractical for lunar habitat operations.	Select low-power components and prioritize energy efficiency in design decisions.
5	Sensor degradation in lunar environment	Radiation exposure and thermal cycling in lunar habitats may degrade sensor performance and reduce signal fidelity.	Ensure electronics and components are rated for lunar environmental conditions.
6	Noisy readings during mission	Differences between lunar habitat and lab conditions could produce unstable or noisy sensor signals.	Conduct thorough laboratory testing and calibration to stabilize signal interpretation.

Appendix 4: Project Timeline

Table 6: HuLC scope timeline

WBS NUMBER	TASK TITLE	START DATE	DUE DATE	DURATION	PCT OF TASK COMPLETE
1	Project Conception and Initiation				
1.1	Proposal paper due	2/25/26	3/4/26	9	100%
1.1.1	Prototype CAD iteration 1	2/1/26	3/4/26	33	100%
1.2	Prototype CAD iteration 2	3/4/26	3/17/26	13	100%
1.3	Bill of Materials (BoM)	3/11/26	3/20/26	9	100%
1.4	BoM and plan faculty review	3/23/2026	3/25/26	2	100%
1.5	Ordering and procurement period	3/25/26	4/6/26	11	100%
1.6	Project assembly and development	4/6/26	4/13/26	7	100%
2	Testing				
	HuLC Finalist teams announced	April--TBA			100%
2.1	Ultrasonic testbed assembly and testing	4/13/26	4/14/26	1	100%
2.2	Fiber Optic testbed assembly and testing	4/14/26	4/15/26	1	100%
2.3	Colorimetric testbed assembly and testing	4/15/26	4/16/26	1	100%
2.4	Triple-system integrated testing	6/1/26	6/3/26	2	20%
3	Reiteration period				
3.1	Mission-readiness assessment	6/3/26	6/4/26	1	0%
3.2	Reiteration of design	6/4/26	6/6/26	2	0%
3.3	Assermbly period	6/7/26	6/8/26	1	0%
3.4	Problem-specific testing period	6/9/26	6/11/26	2	0%
3.5	Improvement period	6/11/26	6/12/26	1	0%
3.6	Status report for faculty	6/13/26	6/18/26	5	0%
4	Project Performance/Monitoring				
4.1	Deliverables prepared for HuLC forum	6/15/26	6/18/26	3	0%
	HuLC forum	6/22/26	6/25/26	1	0%

Appendix 5: References

National Space Policy Council. "A Sustained Lunar Presence." NASA, April 2020. https://www.nasa.gov/wp-content/uploads/2020/08/a_sustained_lunar_presence_nspc_report4220final.pdf

Rojdev, K., et al. "Structural Material Options for a Lunar Habitat." NASA Technical Reports Server, 2009. https://ntrs.nasa.gov/api/citations/20090029953/downloads/20090029953.pdf

Xiao, F., Hulsey, J.L., Balasubramanian, R. "Fiber optic health monitoring and temperature behavior of bridge in cold region." *Structural Control and Health Monitoring*, 24(11), e2020, 2017. https://doi.org/10.1002/stc.2020

Juwet, M., et al. "Fiber Bragg Grating sensors in space environments." *npj Microgravity*, 2024. https://link.springer.com/article/10.1007/s44461-025-00003-6

"Recent Advances in Colorimetric Sensors for Environmental Monitoring." *ACS Nano*, American Chemical Society, 2020. https://pubs.acs.org/doi/10.1021/acsnano.0c05916

"Recent Developments in Colorimetric Detection of Environmental Contaminants." *New Journal of Chemistry*, Royal Society of Chemistry, 2016. https://pubs.rsc.org/en/content/articlelanding/2016/nj/c6nj02092e

"Advances in Fiber Optic Sensor Systems for Environmental Monitoring." *Sensors and Actuators A: Physical*, ScienceDirect, 2025. https://www.sciencedirect.com/science/article/pii/S1350448725001799

"Nanopigment Sensor Tracks pH Changes in Ten Seconds." *Phys.org*, February 2026. https://phys.org/news/2026-02-nanopigment-sensor-tracks-ph-ten.html

Texas Instruments. "Op Amp Precision Design Guide." Application Report SBOA567. https://www.ti.com/lit/ab/sboa567/sboa567.pdf

A. Bulletti, E. M. Merlo, and L. Capineri, “Analysis of the accuracy in impact localization using piezoelectric sensors for Structural Health Monitoring with multichannel real-time electronics,” 2020 IEEE 7th International Workshop on Metrology for AeroSpace (MetroAeroSpace), Pisa, Italy, 2020, pp. 480–484, doi: 10.1109/MetroAeroSpace48742.2020.9160275.

NASA. “Weather on the Moon.” NASA Science, National Aeronautics and Space Administration. https://science.nasa.gov/moon/weather-on-the-moon/

NASA. “Lunar Planetary Wireless Network Spec Sheet.” National Aeronautics and Space Administration, Sept. 2024. https://www.nasa.gov/wp-content/uploads/2024/09/18-lunar-planetary-wireless-network-spec-sheet-508.pdf?emrc=da7acc

NASA. “Advanced Modular Power Systems for Space Applications.” NASA TechPort, Project 102925. https://techport.nasa.gov/projects/102925